Journal of the Korean Chemical Society
2012, *Vol. 56, No. 4*
Printed in the Republic of Korea
http://dx.doi.org/10.5012/jkcs.2012.56.4.484

Preparation, Characterization and Catalytic Activity of Tin Dioxide and Zero-Valent Tin Nanoparticles

H. R. Pouretedal*, A. Shafeie†, and M. H. Keshavarz
Faculty of Applied Chemistry, Malek-ashtar University of Technology, Shahin-Shahr, Iran.
**E-mail: HR_POURETEDAL@mut-es.ac.ir*
†Department of Chemistry, Islamic Azad University, Shahreza Branch, Shahreza, Iran
(Received January 18, 2012; Accepted June 4, 2012)

ABSTRACT. The tin (IV) oxide nanoparticles are prepared by controlled precipitation method and calcined at temperatures of 200-600 °C. The prepared SnO_2 nanoparticles characterized by XRD patterns, TEM image, IR and UV-Vis spectra. The XRD patterns and TEM image show the tetragonal structure and spherical morphology for SnO_2 nanoparticles, respectively. The photocatalytic activity of the prepared SnO_2 nanoparticles studied in degradation reaction of methylene blue (MB). The results show the size of nanoparticles, band-gap energy and photocatalytic activity of SnO_2 depends on the calcinations temperature. The SnO_2 nanoparticles calcined at 500 °C indicated the highest photoreactivity. Also, the zero-valent tin (ZVT) nanoparticles with tetragonal structure are prepared by a reducing agent and used as a catalyst in degradation of MB. In basic pH of 11, the degradation >95% of MB at time 150 min obtained at presence of ZVT nanoparticles.

Key words: SnO_2, Sn, Nanoparticles, Methylene blue, Photocatalyst

INTRODUCTION

Nanometer range semiconducting materials have been a subject of intense study for last several years due to their size dependent physical and chemical properties below a critical size characteristic of the material.[1,2] Photocatalytic property is a interesting property that exhibited by these nanocrystals. This property is size quantization effect which arise due to the increasing quantum confinement of the electrons and holes with diminishing size of the crystallites and the consequent changes in the electronic structures.[3-5]

The performance and application of semiconductor photocatalyst are largely based on how much its electronic structure and photoinduced charge property at the surface or interface are realized.[5] The studies on the effects of some factors, such as material size, phase composition, structure and dopant species, on the properties of photoinduced charges, including charge transfer behavior and surface states, are of very significance to the preparation and application of semiconductor materials.[4]

Semiconductor photocatalysis has attracted increasing attention as an effective technique to eliminate the pollutants in air and wastewater. While many efforts have been made to put this technique into commercial application, many problems arise, such as the fast recombination rate of the photoexcited electron-hole pairs, which is the key factor in the process of semiconductor photocatalysis.[6,7] Therefore, there has been much interest in lowering the recombination rate of electron-hole pairs in order to improve the photocatalytic efficiency of semiconductor photocatalysts.[8]

Tin (IV) oxide has been a widely studied material over decades because of its wide range of applications as gas sensors, heat mirrors, and transparent electrodes for solar cells, opto-electronic devices and in catalysis.[9] Tin dioxide is an *n*-type semiconductor crystallizing in tetragonal rutile structure and having the band-gap of about 3.65 eV at bulk state.[10]

Applications of Sn (0) nanoparticles are in the preparation of metal films, as Li alloy anodes for rechargeable batteries, as precursors to SnO_2 nanoparticles for use as gas sensors and in heterogeneous catalysis.[11,12] However, despite the unique properties of Sn (0) particles in hybrid materials or catalysis, there are only a few reports dealing with their preparation. Evaporation under ultrahigh vacuum of bulk tin followed by condensation of the vapor is by far the most common method for the synthesis of Sn (0) particles.[13,14]

In this work, the production of SnO_2 and zero-valent tin (ZVT) nanoparticles and characterization of prepared nanoparticles is reported. The effect of calcinations temperature studied on the photocatalytic activity of SnO_2 nanoparticles. The bleaching of methylene blue is also

studied in presence of SnO_2 and zero-valent tin (ZVT) nanoparticles.

EXPERIMENTAL

Synthesis of SnO_2 and Sn Nanoparticles

All materials were purchased from Merck and Aldrich Company with high purity and analytical grade. The double distilled water was used to prepare the aqueous solutions.

Tin (IV) chloride ($SnCl_4 \cdot 5H_2O$) and ammonia solution (1:1) with high purity and analytical grade were used as precursor for synthesis of SnO_2 nanoparticles. A controlled precipitation procedure used to prepare the SnO_2 nanoparticles. Firstly, ammonia solution was added to 50 ml of 0.05 M $SnCl_4$ solution drop by drop using a decanter with control of sample pH while the mixture was stirred vigorously at 80 °C temperature. The pH of sample was controlled at pH of 3-4 and heating and stirring of sample was continued duration 2-3 h. The white precipitate of $Sn(OH)_4$ was then centrifuged at 3000-4000 rpm, washed with water and ethanol several times. The $Sn(OH)_4$ nanoparticles were treated by heating in temperature of 80 °C for about 4 h. Finally, the white SnO_2 powders were calcined in an oven at temperatures of 200-600 °C for about 2 h and then stored for further use.

The zero-valent tin nanoparticles were prepared by $SnCl_2$ as starting material, sodium borohydride ($NaBH_4$) as reducing agent and Tween80 as surfactant. Sodium borohydride solution (0.06 M) was added to a solution of 0.1 %w/w $SnCl_2$ and 0.2 %w/w of Tween80 so that one drop was added each of 3-4 s. The Sn nanoparticles was removed by centrifuge with 3000-4000 rpm and then washed with water and ethanol several times and dried at 50-60 °C at time 2-3 h.

Characterization of Nanoparticles

The prepared nanoparticles characterized by using X-ray diffraction (XRD) patterns, IR spectra, UV-Vis spectra and TEM images. An X-ray Diffractometer Bruker D8ADVANCE Germany with anode of Cu (wavelength of 1.5406Å of Cu K_α) and filter of Ni apply to record the XRD patterns of nanosized powders. The nanoparticles size was estimated by a JEOL JEM-1200EXII transmission electron microscope (TEM) operating at 120 kV. The supporting grids were formvar-covered, carbon-coated, 200-mesh copper grids. IR-spectra of SnO_2 nanoparticles in range 4000-400 cm^{-1} were recorded by using *Nicolet Impact 400D FT-IR Spectrophotometer*. UV-Vis Spectrophotometer Carry-100 used to record absorption spectra of synthesized SnO_2 in range of 200-500 nm. B.E.T (Brunauer-Emmett-Teller) surface area of nanoparticles was determined by using Monosorb Quantochorom.

Catalytic Activity of Nanoparticles

The photocatalytic activity of SnO_2 nanoparticles studied in the degradation reaction of methylene blue (MB). A photocatalytic reactor system with a mercury low pressure lamp (70 W) with λ_{max}=332 nm and light intensity 22 W/m^2 used to measure photoactivity of SnO_2 nanoparticles. The lamp and the tube were then immersed in the photoreactor cell with a light path of 3.0 cm. The photoreactor was filled with 50 ml sample contain 10.0-50.0 mg/L MB and 0.0-1.2 g/L nanoparticles of SnO_2. The temperature of photoreactor was kept at 25 °C with a water-cooled jacket on its outside. A magnetic stirrer applied to ensure that the suspension of the heterogeneous catalyst is uniform during the degradation. Batch experiments were also performed to study the effect of ZVT nanoparticles in degradation of MB. Dye solution (10-50 mg/L) was prepared in deionized water. A 100 mL of MB solution was poured into a 250-mL Erlenmeyer flask and 0.8 g/L of ZVT nanoparticles was added.

The degraded samples collected at regular intervals, filtered through Millipore membrane filters, and centrifuged to remove the particles. The collected samples were analyzed to measure the absorbance of dye by using a UV-Vis spectrophotometer. The decrease of absorbance value of samples at λ_{max} of dye (625 nm) in certain time intervals shows the rate of degradation efficiency (%D) and calculated by Eq (1):

$$\%D = 100\times[(C_o-C_t)/C_o] = 100\times[(A_o-A_t)/A_o] \quad (1)$$

In Eq (1), C_o and C_t are the initial concentration and concentration of dye at time t, respectively, and A_o and A_t are the initial absorbance and absorbance of dye at time t, respectively.

Kinetic Study of Catalyzed Degradation

The simplified pseudo-first order kinetic model of Langmuir-Hinshelwood (Eq. 2) use to calculate the apparent rate constant of degradation process of dye at initial concentrations 10, 20, 30, 40 and 50 mg/L at pH 11.

$$\ln(C_o/C_t) = kKt = K_{app}t \quad (2)$$

In Eq. (2), C is concentration of the dye (mg/L), t is degradation time (min), k is reaction rate constant (min^{-1}), K is the adsorption coefficient of the dye onto the catalyst par-

ticles (L/mg) and k_{app} is the apparent rate constant (min^{-1}).

The photocatalytic activity of prepared SnO_2 was also studied under sunlight irradiation and also compared to commercial SnO_2. The recovery of catalysts and reusability of them were studied at optimum conditions. Also, the MB bleaching catalyzed by nanosized SnO_2 was studied in presence of chloride, bromide, iodide, carbonate, sulfate, phosphate, nitrate anions and magnesium and calcium cations as like a real sample.

RESULTS AND DISCUSSION

Characterization of SnO_2 and Zero-valent Tin Nanoparticles

Figs. 1A-1D show the XRD patterns of SnO_2 nanoparticles that are calcined at temperatures of 300, 400, 500 and 600 °C in time 2 h, respectively. As seen, in all temperatures, the calcined SnO_2 particles show the diffraction peaks of (110), (101), (200), (111), (211), (220), (002), (311), (112), (301), (202) and (321) at 2q of 26.8, 33.9, 37.9, 39.0, 51.8, 54.8, 57.7, 61.8, 64.8, 66.0, 71.2 and 78.6°, respectively. Which matches well with JCPDS card # 41-1445 and structure of the crystal is found to be Cassiterite type tetragonal of SnO_2 crystal.[10,11,15] But, the crystalinity of particles as well as the particles size increase with increasing of calcinations temperature. The XRD patterns show the decreasing of FWHM and thus increasing of particles size of SnO_2 with increasing of calcinations temperature from 300 to 600 °C. The average crystallite size of the tin dioxide crystal calcined at 300, 400, 500 and 600 °C was calculated from Debye-Scherrer formula[15] and found 2.46, 3.48, 5.21 and 8.31 nm, respectively. The TEM micrograph of SnO_2 nanoparticles calcined at 500 °C is shown in *Fig*. 2 that reveals the morphology and particles size. The monodispersed particles with spherical shape and size <25 nm with an equable distribution except for a little aggregated particulate, is observed in TEM image. On the other hand, the TEM photographs show that tin (IV) oxide powder is nanometer scale, which is in reasonable agreement with the results obtained from the XRD patterns.

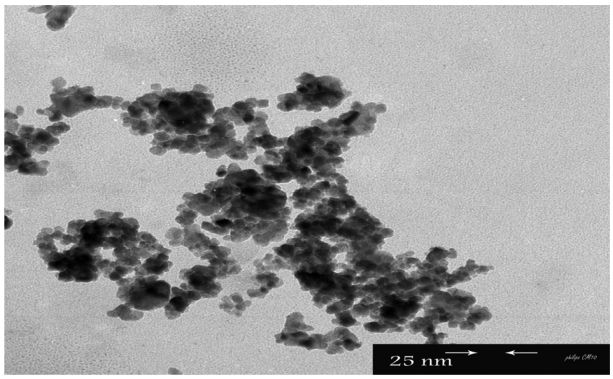

***Fig*. 2.** TEM image of SnO_2 nanoparticles calcined at 500 °C.

The FT-IR spectra of SnO_2 nanoparticles (*Fig*. 3) show the bands of 600-700 cm^{-1} that are assigned to the antisymmetric Sn-O-Sn stretching mode of the surface-bridging of oxide.[16] The UV-Vis spectra of SnO_2 calcined at temperatures of 400, 500 and 600 °C are shown in *Fig*. 4.

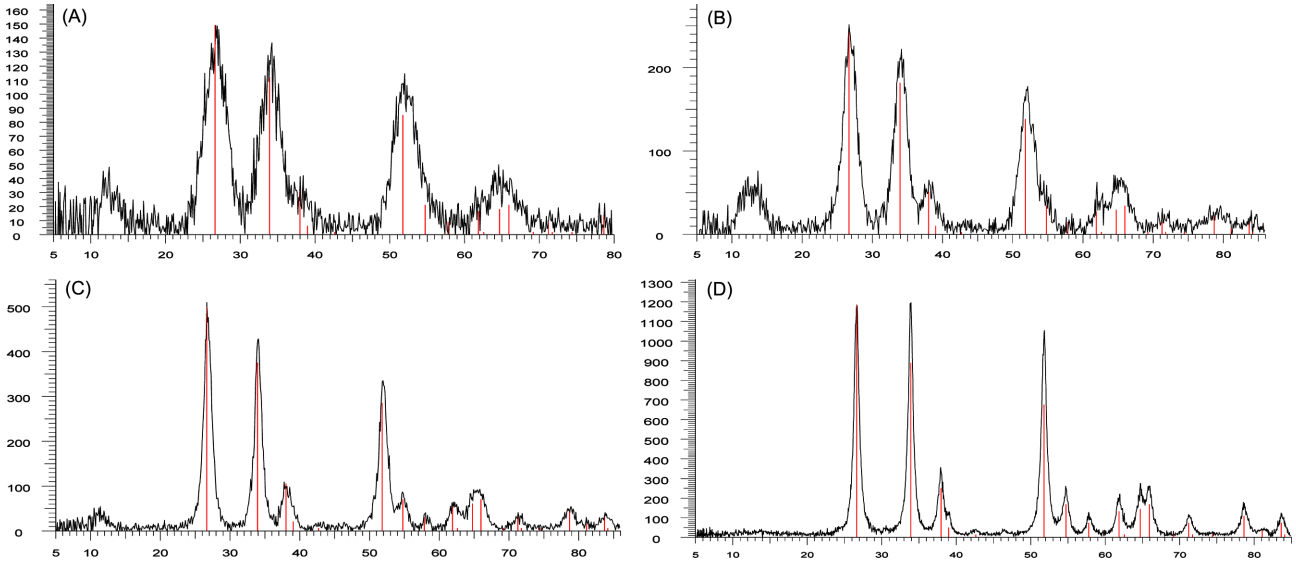

***Fig*. 1.** (A) XRD pattern of SnO_2 nanoparticles calcined at 300 °C, (B) XRD pattern of SnO_2 nanoparticles calcined at 400 °C, (C) XRD pattern of SnO_2 nanoparticles calcined at 500 °C. (D) XRD pattern of SnO_2 nanoparticles calcined at 600 °C.

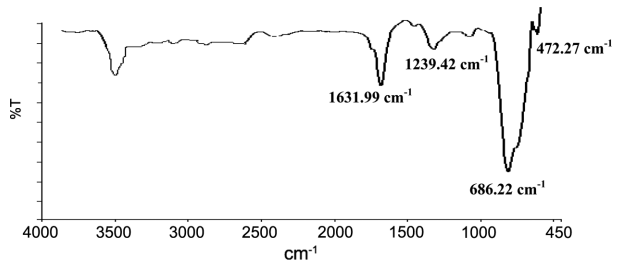

***Fig.* 3.** FT-IR spectra of SnO_2 calcined at 500 °C.

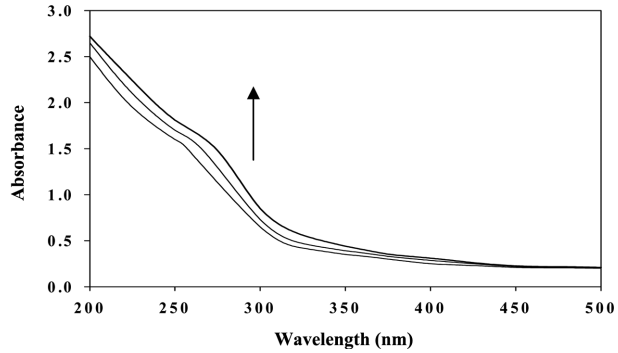

***Fig.* 4.** The UV-Vis spectra of SnO_2 nanoparticles calcined at 400, 500 and 600 °C from down to up.

The red-shift in absorption edge is observed with increasing of temperature. So that, the wavelength of absorption edge is observed at 262, 268 and 275 nm for SnO_2 calcined at temperatures of 400, 500 and 600 °C, respectively.[17,18]

Figs. 5 and 6 indicate the XRD pattern and TEM micrograph of zero-valent Sn nanoparticles, respectively. The XRD pattern show diffraction peaks that are indexed to a tetragonal cell for tin particles (JCPDS #04-0673).[19,20] The crystallite size of tin nanoparticles with Scherrer formula is estimated to be 16.62 nm. The TEM micrograph is also confirmed the formation of tin nanoparticles with size less of 20 nm by reduction of Sn^{2+} ions by $NaBH_4$ at presence of Tween80. Also, the B.E.T analysis indicated that the surface area of zero-valent tin nanoparticles is 15.8 m^2/g.

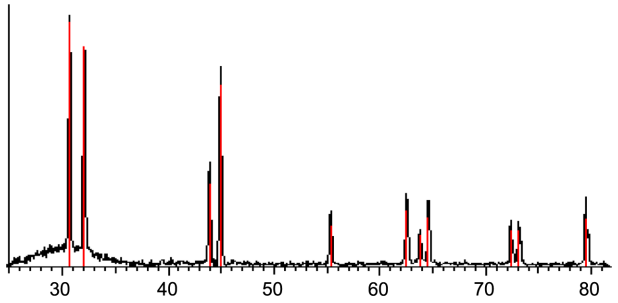

***Fig.* 5.** XRD pattern of zero-valent tin nanoparticles.

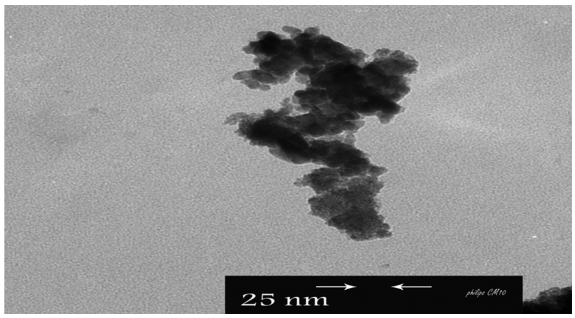

***Fig.* 6.** TEM image of zero-valent tin nanoparticles.

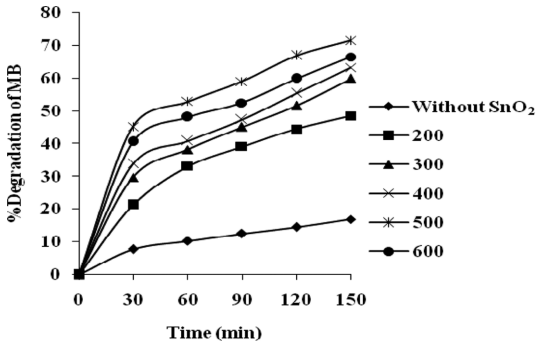

***Fig.* 7.** Effect of calcination temperature (°C) on the photocatalytic activity of SnO_2 nanoparticles.

Photocatalytic Activity of SnO_2 Nanoparticles

The photocatalytic activity of SnO_2 can be dependent on the preparation conditions such as time and temperature of treatment and calcination process. The effect of calcination temperature on the photocatalytic activity of SnO_2 in methylene blue degradation is shwon in *Fig*. 7. The conditions are 0.1 g/L catalyst, pH of 7 and MB of 10 mg/L. As seen, the highest photocatalytic activity is due to SnO_2 nanoparticles calcined at 500 °C. As mentioned (*Figs*. 1A to 1D), the crystallinity and powder size of SnO_2 nanoparticles increase with increasing of calcinations temperature. On the other hand, the band-gap energy is calculated 4.72, 4.62 and 4.50 eV for SnO_2 nanoparticles calcined at temperatures of 400, 500 and 600 °C, respectively (*Fig*. 4). The band-gap energy of semiconductors is related to their photocatalytic activity for phtodegradation of pollutants. The greater of redox potential of the photogenerated electron-hole pairs is due to the larger of band-gap energy. Thus, a semiconductor exhibits more redox capacity with increase of band-gap.[21,22] Therefore, the most degradation for MB is seen in presence of SnO_2 calcined at 500 °C with band-gap energy of 4.62 eV and size of 5.21 nm. The SnO_2 calcined at 600 °C show the lower activity despite of having the lower band-gap energy. This decrease is related to increasing of par-

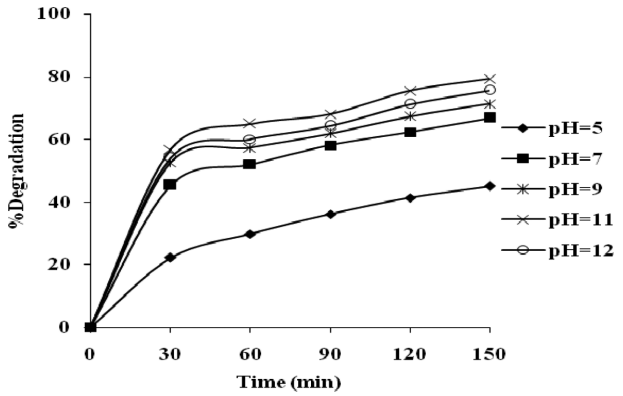

***Fig*. 8.** Effect of samples pH on the photocatalytic activity of SnO_2 nanoparticles.

ticles size and thus the decrease of surface due to agglomeration of them in 600 °C temperature.

The photocatalytic activity of a semiconductor is related to the pH of samples and dosage of it. The effects of pH and amount of SnO_2 nanoparticles are indicated in *Figs*. 8 and 9, respectively. The *Fig*. 8 shows the increasing of photocatalytic activity of SnO_2 nanoparticels with increasing of samples pH. The increasing of pH is due to increase hydroxyl ions concentration to react with the holes and formation hydroxyl radicals. Also, the adsorption of MB molecules with positive charge is occurred on the surface of catalyst in basic solutions because the negative charge of SnO_2 with pH of isoelectric point of 3.5.[22] However, the degradation of MB is inhibited when the pH is greater than 11. Because the hydroxyl ions compete with dye molecules in adsorption on the surface of catalyst.[23,24] Degradation efficiency at presence of 0.1, 0.5, 0.8, 1.0 and 1.2 g/L is obtained 78.6, 88.7, 93.5, 89.1 and 84.2, respectively. As seen, the optimized value of SnO_2 nanoparticles is 0.8 g/L. The active sites and density of particles in the area of illumination are increased with increasing of concentration of catalyst in the photodegradation process.[25,26] But, at higher catalyst loading of 0.8 g/L, the activated particles deactivate by agglomeration. Also, the decrease of radiation penetration and increase of radiation scattering occur at higher catalyst loading.

Because the influence of many factors and even their mutual effects, the heterogeneous photocatalysis reaction is complicated process. However, the pseudo-first-order rate equation of Langmuir–Hinshelwood (Eq. 2) is used to determine the apparent rate constant, k_{app}, of MB photodegradation catalyzed by SnO_2 nanoparticles.[27] The apparent rate constants are obtained at range of 10-50 mg/L of methylene blue and collected in *Table* 1. The regression

***Table* 1.** The apparent rate constants (k_{app}, min^{-1}) and regression coefficients (R^2) of methylene blue degradation catalyzed by SnO_2 and zaro-valent Sn nanoparticles calcined at 500 °C

C_o, mg/L	SnO_2 nanoparticles		Zero-valent Sn nanoparticles	
	k_{app}	R^2	k_{app}	R^2
10	23.3×10^{-3}	0.9553	15.4×10^{-3}	0.9553
20	14.7×10^{-3}	0.9824	9.6×10^{-3}	0.9824
30	9.0×10^{-3}	0.9914	6.2×10^{-3}	0.9914
40	6.4×10^{-3}	0.9678	4.0×10^{-3}	0.9678
50	5.8×10^{-3}	0.9812	2.1×10^{-3}	0.9812

coefficients (R^2) of Langmuir-Hinshelwood kinetic model also indicated in *Table* 1. As seen, the apparent rate constant decrease with increasing of the initial concentration of MB. The decrease of apparent rate constant is due from two reasons: i) increasing the probability of absorption of photons by pollutant molecules and decrease to reach of them to surface of catalyst, ii) increasing of pollutant molecules adsorbed on the surface of catalyst and decrease the active sites to generate of radicals.[28,29]

Photocatalytic activity of prepared SnO_2 nanoparticles studied also under sunlight irradiation in optimized conditions. The degradation efficiency of MB was 92.7% in time 150 min with apparent rate constant of 21.6×10^{-3} min^{-1}. As a result, the prepared tin (IV) oxide shows photocatalytic activity under sunlight irradiation as well UV-irradation.

The photocatalytic activity of SnO_2 nanoparticles investigated in presence of ions of Ca^{2+}, Mg^{2+}, Cl^-, Br^-, I^-, CO_3^{2-}, NO_3^-, SO_4^{2-} and PO_4^{3-} with concentration of 1000 mg/L as real samples. The effect of each ion on the nanosized SnO_2 activity is shown in *Fig*. 9. However, the photocatalytic activity of SnO_2 nanoparticles diminished in a real sample contains cations and anions. This reduction is due to scavenger effect of active radicals by cations and anions.[4]

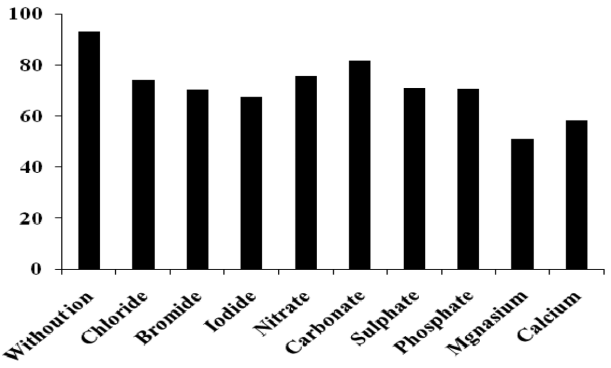

***Fig*. 9.** The effect of several ions on the photocatalytic activity of SnO_2 nanoparticles.

Also, the catalytic activity of tin dioxide nanoparticles is compared to commercially SnO_2 with purity of 99.7%. The degradation of 63.4% of MB is obtained at presence of commercially SnO_2 powder. This reduction of degradation efficiency can be due to difference of surface area and band-gap of SnO_2 nanoparticles and SnO_2 powder. So that, B.E.T (Brunauer-Emmett-Teller) surface area of prepared nanoparticles is obtained 258.3 m^2/g in comparison of 132.6 m^2/g of SnO_2 powder. The reusability of SnO_2 nanoparticles studied in four-cycles. In each cycle, the nanoparticles separated, washed with water and ethanol and dried at 80 °C and used in next cycles. The D% values obtained 97.0, 93.7, 89.7 and 82.6% in order of four-cycles.

Catalytic Activity of Zero-valent Tin Nanoparticles

The use of zero-valent metal particles such as Sn for decontamination of common soil and water contaminants has been the subject of many studies.[30] Synthesis of zero-valent tin (ZVT) nanoparticles was achieved by reaction $NaBH_4$ and $SnCl_2$ according to the following equation:

$$2Sn^{2+}+BH_4^{+}+2H_2O\rightarrow 2Sn(0)+BO_2^{-}+4H^{+}+2H_2\,(g) \quad (3)$$

The bleaching of MB solution studied at presence of 0.8 g/L of ZVT nanoparticles and pH 11 like as the optimum conditions in photodegradation reaction. The pseudo first-order rate constants (k_{app}) of MB degradation by ZVT nanoparticles are calculated using Eq. (2) and indicated in *Table* 1. As seen, the rate constants of MB degradation catalyzed by SnO_2 photocatalyst and ZVT nanoparticles are near to each other. The MB degradation is obtained 97.8 and 92.1% in presence of SnO_2 and Sn nanoparticles, respectively, in duration of 150 min. Thus, reactivity of ZVT nanoparticles in MB degradation process is comparable with photocatalytic activity of SnO_2 nanoparticles in photodegradation reaction of dye in spite of different in degradation mechanism. The holes and electrons are produced by SnO_2 semiconductor under irradiation and the formation of hydroxyl radicals particularly in basic solution apply as an active species in degradation of MB.[31] While, zero-valent tin is a strong reducing agent in basic solutions with E^o=-0.91 and -0.93 V for Sn(II) to Sn(0) and Sn(IV) to Sn(II), respectively (Eq. 4). Furthermore, the most important factor that influences on k_{app} is the surface area of the zero-valent metal.[32]

$$Sn(OH)_6^{2-} \xrightarrow{-0.93} SnO_2H^{-} \xrightarrow{-0.91} Sn \quad (4)$$

This means that it can act as an electron donor that due to reduction of MB molecules in basic solution. The methylene blue is a redox indicator with blue color in oxidized form and colorless in reduced form. The reduction of MB is occurred in acidic solutions and this reduction is due to reduction of absorbance at λ_{max} of it in visible region. While, in basic solution (pH=11) and in presence of ZVT nanoparticles, the MB molecules degrade and the reduction of absorbance in wavelength ranges of 200-300 and 600-700 nm is observed in UV-Vis spectra similar to variations of MB absorption spectra in photodegradation reaction. Thus, Sn (0) nanoparticles as well SnO_2 nanoparticles in photodegradation could be due to destruction of a dye pollutant such as MB.

CONCLUSION

The activity of SnO_2 as a photocatalyst is dependent on the calcinations temperature, dosage of it and pH of samples. Because, the calcinations temperature influence on the band-gap energy and size of particles. The zero-valent tin as reducing agent can be due to degradation of methylene blue in basic solution. In the same conditions of nanoparticles (0.8 g/L of catalyst) and sample pH of 11, the SnO_2 nanoparticles and zero-valent Sn nanoparticles show similar and attractive activity in degradation of methylene blue as a dye pollutant.

REFERENCES

1. Robert, D. *Catal. Today* **2007**, *122*, 20.
2. Jing, L.; Fu, H.; Wang, B.; Wang, D.; Xin, B.; Li, S.; Sun, J. *Appl. Catal., B: Environ.* **2006**, *62*, 282.
3. Jing, L.; Wang, D.; Wang, B.; Li, S.; Xin, B.; Fu, H.; Sun, J. *J. Mol. Catal., A: Chem.* **2006**, *244*, 193.
4. Augugliaro, V.; Litter, M.; Palmisano, L.; Sori, J. *J. Photochem. Photobiol. C* **2006**, *7* 127.
5. Liotta, L. F.; Gruttadauria, M.; Di Carlo, G.; Perrini, G.; Librando, V. *J. Hazard. Mater.* **2009**, *162*, 588.
6. Pouretedal, H. R.; Norozi, A.; Keshavarz, M. H.; Semnani, A. *J. Hazard. Mater.* **2009**, *162*, 674.
7. Pouretedal, H. R.; Eskandari, H.; Keshavarz, M. H.; Semnani, A. *Acta Chim. Slov.* **2009**, *56*, 353.
8. Wang, H.; Baek, S.; Lee, J.; Lim, S. *Chem. Eng. J.* **2009**, *146*, 355.
9. Dhage, S. R.; Gaikwad, S. P.; Samuel, V.; Ravi, V. *Bull. Mater. Sci.* **2004**, *27*, 221.
10. Kandjani, A. E.; Salehpoor, P.; Tabrizi, M. F.; Arefian, N. A.; Vaezi, M. R. *Mater. Sci.-Poland* **2010**, *28*, 377.
11. Balan, L.; Schneider, R.; Billaud, D.; Ghanbaj, J. *Mater. Lett.* **2005**, *59*, 1080.
12. Lee, K. T.; Jung, Y. S.; Oh, S. M. *J. Am. Chem. Soc.* **2003**, *125*, 5652.
13. Bottani, C. E.; Li Bassi, A.; Tanner, B. K.; Stella, A.; Tognini, P.; Cheyssac, P.; Kofman, R. *Mater. Sci. Eng., C,*

Biomim. Mater., Sens. Syst. **2001**, *15*, 41.
14. Depero, L. E.; Bontempi, E.; Sangaletti, L.; Pagliara, S. *J. Chem. Phys*. **2003**, *118*, 1400.
15. Krishnakumar, T.; Jayaprakash, R.; Parthibavarman, M.; Phani, A. R.; Singh, V. N.; Mehta, B. R. *Mater. Lett*. **2009**, *63*, 896.
16. Anandan, K.; Rajendran, V.; *J. Non-Oxide Glasses* **2010**, *2*, 83.
17. Zhang, M.; An, T.; Hu, X.; Wang, C.; Sheng, G.; Fu, J. *Appl. Catal.*, *A* **2004**, *260*, 215.
18. Jiang, L.; Sun, G.; Zhou, Z.; Sun, S.; Wang, Q.; Yan, S.; Li, H.; Tian, J.; Guo, J.; Zhou, B.; Xin, Q. *J. Phys. Chem. B* **2005**, *109*, 8774.
19. Zhao, Y.; Zhang, Z.; Dang, H. *Mater. Sci. Eng. A* **2003**, *359*, 405.
20. Noh, M.; Kim, Y.; Kim, M. G.; Lee, H.; Kim, H.; Kwon, Y.; Lee, Y.; Cho, J. *Chem. Mater.* **2005**, *17*, 3320.
21. Gu, F.; Wang, S. F.; Leu, M. K.; Qi, Y. X.; Zhou, G. J.; Xu, D.; Yuan, D. R. *Inorg. Chem. Commun.* **2003**, *6*, 882.
22. Rodriguez-Santiago, V.; Fedkin, M. V.; Wesolowski, D. J.; Rosenqvist, J.; Lvov, S. N. *Langmuir* **2009**, *25*, 8101.
23. Pouretedal, H. R.; Hosseini, M. *Acta Chim. Slov.* **2010**, *57*, 415.
24. Pouretedal, H.R.; Kadkhodaie, A. *Chin. J. Catal*. **2010**, *31*, 1328.
25. Nezamzadeh-Ejhieh, A.; Hushmandrad, S. *Appl. Catal., A* **2010**, *388*, 149.
26. Nezamzadeh-Ejhieh, A.; Salimi, Z. *Appl. Catal., A* **2010**, *390*, 110.
27. Wang, K.; Zhang, J.; Lou, L.; Yang, S.; Chen, Y. *J. Photochem. Photobiol. A* **2004**, *165*, 201.
28. Pouretedal, H. R.; Keshavarz, M. H. *J. Alloys Comp.* **2010**, *501*, 130.
29. Kudo, A.; Niishiro, R.; Iwase, A.; Kato, H. *Chem. Phys*. **2007**, *339*, 104.
30. Lin, C. J.; Liou, Y. H.; Lo, S. L. *Chemosphere* **2009**, *74*, 314.
31. Hoffmann, M. R.; Martin, S. T.; Choi, W.; Bahnemannt, D. W. *Chem. Rev.* **1995**, *95*, 69.
32. Satapanajaru, T.; Chompuchan, C.; Suntornchot, P.; Pengthamkeerati, P. *Desalination* **2011**, *266*, 218.